Published in final edited form as:

Circ Arrhythm Electrophysiol. 2016 April ; 9(4): . doi:10.1161/CIRCEP.115.003926.

Transcatheter Myocardial Needle Chemoablation during Real-Time MRI: A New Approach to Ablation Therapy for Rhythm Disorders

Toby Rogers, BM BCh MRCP[1], **Srijoy Mahapatra, MD**[2], **Steven Kim, MS**[3], **Michael A. Eckhaus, VMD**[3], **William H. Schenke, BA**[1], **Jonathan R. Mazal, MS**[1], **Adrienne Campbell-Washburn, PhD**[1], **Merdim Sonmez, PhD**[1], **Anthony Z. Faranesh, PhD**[1], **Kanishka Ratnayaka, MD**[1,4], and **Robert J. Lederman, MD**[1]

[1]Cardiovascular and Pulmonary Branch, Division of Intramural Research, National Heart Lung and Blood Institute, National Institutes of Health, Bethesda, MD

[2]St Jude Medical, St Paul, MN

[3]Division of Veterinary Resources, National Institutes of Health, Bethesda, MD

[4]Department of Cardiology, Children's National Medical Center, Washington, DC

Abstract

Background—Radiofrequency ablation for ventricular arrhythmias is limited by inability to visualize tissue destruction, by reversible conduction block resulting from edema surrounding lesions, and by insufficient lesion depth. We hypothesized that transcatheter needle injection of caustic agents doped with gadolinium contrast under real-time magnetic resonance imaging (MRI) could achieve deep, targeted and irreversible myocardial ablation which would be immediately visible.

Methods and Results—Under real-time MRI guidance, ethanol or acetic acid was injected into the myocardium of 8 swine using MRI-conspicuous needle catheters. Chemoablation lesions had identical geometry by *in vivo* and *ex vivo* MRI as well as histopathology, both immediately and after 12(7–17) days. Whereas ethanol caused stellate lesions with patchy areas of normal myocardium, acetic acid caused homogeneous circumscribed lesions of irreversible necrosis. Ischemic cardiomyopathy was created in 10 additional swine by sub-selective transcoronary ethanol administration into non-contiguous territories. After 12(8–15) days, real-time MRI guided chemoablation — with 2–5 injections to create a linear lesion —successfully eliminated the isthmus and local abnormal voltage activities.

Conclusions—Real-time MRI guided chemoablation with acetic acid enabled the intended arrhythmic substrate, whether deep or superficial, to be visualized immediately and ablated

Correspondence: Robert J. Lederman, MD, National Heart Lung and Blood Institute, National Institutes of Health, Building 10, Room 2c713, Bethesda, MD 20892-1538, Tel: +1-301-402-6769, lederman@nih.gov.

Disclosures: NIH and Siemens have a collaborative research and development agreement. SM and SK are employees of St Jude Medical. No other author has a financial conflict of interest related to this work.

Journal Subject Terms: Catheter Ablation and Implantable Cardioverter-Defibrillator; Magnetic Resonance Imaging (MRI); Cardiomyopathy; Catheter-Based Coronary and Valvular Interventions; Animal Models of Human Disease

irreversibly. In an animal model of ischemic cardiomyopathy, obliteration of a conductive isthmus both anatomically and functionally, and abolition of local abnormal voltage activities in areas of heterogeneous scar was feasible. This represents the first report of MRI guided myocardial chemoablation, an approach that could improve efficacy of arrhythmic substrate ablation in the thick ventricular myocardium.

Keywords

ventricular tachycardia; electrophysiology; ablation; intervention; magnetic resonance imaging; interventional MRI; cardiac electrophysiology; radiofrequency ablation; chemoablation

Introduction

Radiofrequency ablation for rhythm disorders is limited by the inability instantaneously to visualize and monitor ablation lesions, and by the mismatch between immediate injury and irreversible conduction block[1]. Magnetic resonance imaging (MRI) thermometry only approximates the extent of irreversible lesions[2]. Late gadolinium enhancement MRI (LGE) correlates with histological lesion volume[3] but can only be performed once per procedure and is not a surrogate for real-time lesion monitoring during ablation. Furthermore, scar size by LGE several months post-ablation is up to 50% smaller than that measured immediately post-ablation[4]. Not only does the lesion contract during fibrotic healing, but LGE after radiofrequency energy injury probably reflects both the necrotic core and enhancement of a surrounding edematous penumbra.

Radiofrequency ablation for ventricular tachycardia (VT) is further limited by the mismatch between thickness of left ventricular (LV) myocardium and shallowness of radiofrequency lesions[5]. Critical peri-infarct substrate can be deep within the myocardium and difficult to ablate via endocardial or epicardial approaches[6]. Failure to achieve permanent transmural tissue destruction is a common cause of therapeutic failure. MRI tissue characterization techniques can identify pathologic rhythm substrate tissues such as a critical re-entrant isthmus or a peri-infarct slow-conduction heterogeneous zone[7]. Areas of scar tissue by LGE have in animals shown close similarity to electroanatomic voltage maps[8]. Trans-catheter MRI guided radiofrequency ablation of atrial tissue has been reported in early human studies[9, 10].

Chemoablation is already used for trans-coronary interventricular septal ablation in patients with hypertrophic cardiomyopathy[11], in the viscera for tumour ablation[12], and through the vein of Marshall for atrial fibrillation[13]. Caustic agents such as ethanol or acetic acid cause coagulative necrosis, followed by late fibrosis and scarring[14]. These agents are considered safe, because if small quantities reach the blood pool they are immediately diluted down to a harmless concentration. Transarterial[15, 16] or retrograde transvenous[17] chemoablation may allow deeper endocardial lesion creation compared with radiofrequency ablation, but are constrained by the myocardial territories incidentally subtended by the injected vessels and may lead to the destruction of excess tissue. Chemoablation for ventricular arrhythmias by direct endomyocardial injection may overcome these anatomic constraints and may allow more targeted tissue ablation. Pre-clinical feasibility of fluoroscopic or intracardiac

echocardiography guided subendocardial ablation with ethanol has been demonstrated[18], although we are not aware of acetic acid chemoablation in the heart. These techniques remain limited because they do not allow differentiation of target tissues or real-time lesion monitoring.

We hypothesized that real-time MRI would enable substrate-guided myocardial chemoablation. We propose to use MRI to instantaneously visualize arrhythmia substrate and ablative agents doped with gadolinium-based contrast agents. In this report we demonstrate for the first time (1) feasibility of real-time MRI guided myocardial chemoablation in swine; (2) MRI characteristics, macroscopic appearance and histopathology of acute and chronic chemoablation lesions; (3) superior circumscription of myocardial acetic acid chemoablation lesions compared with ethanol lesions; and (4) anatomical and electrical interruption of a conductive isthmus in an animal model of ischemic cardiomyopathy.

Methods

The institutional animal care and use committee approved all procedures, which were performed according to contemporary NIH guidelines. 18 Yorkshire swine with mean body weight 54(46–57)kg were anesthetized with mechanical ventilation. Chemoablation was performed in a clinical 1.5T MRI catheterization suite, equipped with sound-suppression communication headsets and with LCD projectors to display hemodynamics and real-time MRI images at the bedside (Figure 1)[19]. Electroanatomic mapping was performed under X-ray guidance.

Evaluation of chemoablation agents

Gadolinium-based contrast agents can release free gadolinium (Gd^{3+}) at low pH. We therefore tested whether 50% acetic acid (pH 1.9) caused release of free gadolinium from three different commercially available gadolinium-based contrast agents (gadopentetate, Magnevist, *Bayer*; gadofosveset, Ablavar, *Lantheus*; and gadoterate, Dotarem, *Guerbet*). Details of the assay can be found in the supplemental materials.

We characterized ethanol or acetic acid chemoablation lesions in 8 naïve swine. 4 were euthanized immediately and 4 were survived for at least 7 days. 70% ethanol and 50% acetic acid were doped with gadolinium-based contrast agent for MRI conspicuity (2% gadolinium by total volume). Pure ethanol was pre-diluted to 70% with sterile water because in higher concentrations gadopentetate precipitates. 50% acetic acid is the optimal concentration for solid organ tumour ablation[20]. Small aliquots (0.1–0.6mL) of these two solutions were injected into the LV myocardium under real-time MRI guidance. Venous blood was collected before and immediately after chemoablation with acetic acid to assess for effect on systemic pH and anion gap.

MRI guided chemoablation

MRI scanning parameters are detailed in the supplemental materials. Injections into the LV myocardium were delivered using a MRI-conditional deflectable sheath (*Imricor* and *Innotom*) with a passive marker tip and a custom injection needle catheter incorporating

electronics for active visualization. The needle catheter appeared in color on real-time MRI. The sheath was introduced to the LV cavity via transarterial retrograde approach over a Nitinol guidewire (*Nitrex*) under interactive real-time MRI guidance[19]. The needle was navigated to the target myocardium, positioned orthogonally to the endocardial surface (Figure 2) and deployed to a depth of 4mm (or 50% of the myocardial wall thickness). The chemoablation agent was injected slowly in aliquots of 0.1–0.6mL and the needle was withdrawn after 30sec. Chemoablation lesions appeared bright in real-time inversion-recovery MRI as the chemoablation agent doped with gadolinium contrast was injected.

Animal model of ischemic cardiomyopathy

Pigs were pre-treated with amiodarone, aspirin and heparin, and underwent X-ray guided left coronary artery branch balloon occlusion. Obtuse marginal and diagonal arteries were selected for ethanol infarction ensuring that at least one interposed branch (e.g. first diagonal, first obtuse marginal or ramus intermedius) remained intact to create a simulated VT isthmus between the two infarcts. 1–2mL of 70% ethanol / 30% iopamidol contrast was infused through the balloon guidewire lumen to create infarcts. There was no sustained arrhythmia and no mortality. Animals were survived for 12(8–15) days before MRI guided isthmus chemoablation.

Real-time MRI guided isthmus chemoablation

0.2mmol/kg gadopentetate was administered intravenously to the ischemic cardiomyopathy animals. Real-time inversion-recovery MRI identified areas of infarction containing gadolinium contrast. In the first 5 animals, we targeted the normal myocardium interposed between infarcted regions with sequential injections to create a contiguous ablation line to test feasibility of conductive isthmus chemoablation under MRI guidance.

In the other 5 animals, we performed electroanatomic mapping of the LV endocardium ± epicardium using a commercial system and catheters under X-ray guidance (NavX and EnSite Velocity; duo-decapolar Livewire and FlexAbility, *St Jude Medical*) pre- and post-chemoablation. Pericardial access for epicardial mapping was obtained via right atrial appendage exit[21]. Isthmus chemoablation was performed under real-time MRI guidance.

Ex-vivo MRI and histology

After euthanasia hearts were explanted and suspended in agar for high-resolution MRI. Specimens were fixed in 10% formalin, then sectioned and stained with hematoxylin and eosin (H&E) or Masson trichrome.

Statistics

Data were analyzed using SPSS (v19.0, IBM) and are described as mean ± standard deviation if normally distributed, otherwise as median (first and third quartile). Acute and chronic lesion volumes were tested for correlation using Spearman's correlation coefficient. Anion gap and pH pre-and post-chemoablation were compared using paired *t*-tests. A p value <0.05 was considered significant.

Results

Chemoablation lesion histology

In the 8 naïve animals, ethanol lesions exhibited stellate geometry with patchy areas of interposed viable myocardium histologically, whereas acetic acid lesions, exhibited greater homogeneity and more circumscribed borders (Figure 3). Acetic acid lesions were 46% larger than ethanol lesions for the same injection volume. Based on these findings, we performed chronic experiments only using acetic acid. Acute lesions with either agent had a macroscopic area of discoloration with a hemorrhagic center. H&E of acute lesion revealed hypereosinophilia of affected myocardial fibers with mild to moderately pyknotic nuclei and indistinct cross striations, consistent with cellular destruction (Figure 2).

H&E of chronic lesions revealed typical features of fibrosis and replacement of normal myocardial architecture. Masson trichrome revealed a zone of fibroplasia and fibrosis with collagen stained blue, normal myocardial fibers stained red and necrotic myocardial fibers stained purple (Figure 2). Chronic acetic acid lesions were well circumscribed with distinct margins abutting normal myocardium.

Chemoablation lesion appearances by MRI

As gadolinium-doped chemoablation agent was injected into the myocardium, the evolving lesion was visualized in real-time using real-time inversion-recovery MRI (Figure 2). 12(7–17)days after chemoablation, lesions enhanced using LGE after systemic gadolinium contrast administration (Figure 2). Volume of acute acetic acid chemoablation lesions correlated with volume of chronic lesions on LGE (0.78±0.39mL vs. 0.75±0.34mL, Spearman's correlation coefficient=0.72, n=34, $p<0.001$).

Ischemic cardiomyopathy isthmus chemoablation

All 10 animals developed cardiomyopathy (left ventricular end-diastolic volume index 136±17mL/m^2; end-systolic volume index 83±13mL/m^2; ejection fraction 39±5%). After systemic gadolinium contrast administration, infarcts were distinguishable from normal myocardium by LGE or real-time inversion-recovery MRI. Successful transcatheter chemoablation of the isthmus between infarcts was defined as presence of a confluent chemoablation lesion spanning the gap between infarcts and was achieved in all 10 animals with 2–5 separate injections (Figure 1). We mapped LV endocardial ± epicardial voltages before and after MRI guided chemoablation in 5 of these animals. Voltage maps confirmed that a functional ablation line through the isthmus of normal myocardium was successfully created in all 5 animals (Figure 1, Figure 4, and Supplemental Figure S1). Voltages over infarcts were low (0.5–1.5mV), but voltages over chemoablation lesions were even lower (<0.5mV) with clearly defined borders (Figure 5). Local abnormal voltage activities with fragmented slow conduction were abolished with chemoablation (Figure 6).

Safety considerations

Chemoablation did not cause conduction abnormality or sustained tachyarrhythmia in the early post-ablation period. No intramyocardial hematoma, myocardial perforation or rupture, pericardial effusion, pericarditis or tamponade occurred. Linear gadolinium-based contrast

agents (Magnevist and Ablavar) released free gadolinium in 50% acetic acid solution (pH 1.9) within minutes, but did not in 70% ethanol (pH 7). A macrocyclic gadolinium-based contrast agent (gadoterate) did not release any free gadolinium after 60mins incubation in 50% acetic acid (Supplemental Table S1). Chemoablation with acetic acid did not alter serum pH (pre- vs. post-procedure, 7.52±0.17 vs. 7.57±0.15, p=0.34) or anion gap (15.8±3.5 vs. 15.1±3.3, p=0.24; normal range in swine 10–25mEq/L).

Discussion

In this study, we demonstrate for the first time feasibility of real-time MRI guided transcatheter myocardial chemoablation. We show that gadolinium doping of chemoablative agents provides immediate visualization of lesion extent and continuity. Chemoablation lesions correlate with irreversible myocardial injury as evidenced by chronic LGE and histological necrosis. Acetic acid creates homogeneous and well-circumscribed lesions compared with irregularly contoured ethanol lesions. In an animal model of ischemic cardiomyopathy we demonstrate successful substrate-guided chemoablation of a conductive isthmus between two infarcts, with functional ablation confirmed by endocardial and epicardial voltage mapping, and abolition of local abnormal voltage activities in the scar border zones.

Substrate-guided ablation

Conventional electroanatomic mapping relies on surface voltage and activation maps to locate arrhythmia substrate, which can be challenging in the thick-walled LV. In contrast, LGE could afford direct visualization of culprit diseased myocardium for targeted anatomic substrate-guided ablation. Areas of LGE correspond with areas of low endocardial voltage in patients with ischemic cardiomyopathy[22]. Heterogeneous zones, which are a complex mixture of scar and viable myocardium, exhibit abnormal potentials more frequently than dense scar or normal myocardium, and commonly represent the arrhythmic substrate in patients with scar-related VT[7]. MRI-based computational simulation with identification of heterogeneous zones can accurately determine ablation targets[23] and may be used to predict the risk of VT for an individual patient[24]. These may enable entirely substrate-guided ablation in the future. MRI guided chemoablation could also be used to ablate different structures, for example the interventricular septum in patients with LV outflow tract obstruction.

Endocardial vs. epicardial ablation

Endocardial radiofrequency ablation fails to eliminate LV epicardial arrhythmia substrate in many patients. Consequently, epicardial ablation is often required. Sub-xiphoid access to the naïve pericardium and epicardial ablation cause serious complications, including tamponade, abdominal hemorrhage and coronary artery occlusion. Pericardial adhesions and epicardial fat can prevent effective ablation or mislead the operator to believe that effective ablation has been achieved[25]. In contrast, transcatheter needle chemoablation achieves full-thickness ablation from the endocardial surface, avoiding the need for epicardial access. Needle catheters have also been used to deliver radiofrequency energy deeper into the myocardium[26].

Chemoablation is not dependent on catheter tip contact force, and is not subject to steam pop and coagulum embolization, though these problems appear less common with modern irrigated radiofrequency ablation catheters. Because chemoablation does not appear to create an edematous penumbra, it is unlikely to cause reversible conduction block, as does radiofrequency ablation.

Choice of chemoablation agent

Bioenzymatic myocardial ablation has been reported through topical epicardial application of collagenase-soaked sponges that homogenized patchy scar, but the result is not instantaneous and it is not clear whether transmural penetration of the enzyme is achievable[27]. We tested ethanol and acetic acid, the two most commonly used agents for tumour chemoablation in other organs. Based on our bench top and pre-clinical experiments, we favored acetic acid for the following reasons: (1) it has been used safely in humans; (2) it achieved tissue necrosis with smaller injectate volumes compared with ethanol, reducing the risk of extravasation; (3) lesions within the myocardium were more homogenous, well-circumscribed and without patchy interposed viable tissue, an observation that corroborates prior reports using ethanol in the heart and other organs; and (4) we did not observe a change in serum pH or anion gap with acetic acid in swine. We confirmed in a bench top assay that a macrocyclic gadolinium-based contrast agent, unlike linear agents, does not release free gadolinium after incubation in 50% acetic acid. Based on the dissociation half-lives ($T_{1/2}$) at low pH of the available macrocyclic contrast agents, we recommend gadoterate ($T_{1/2}$ 26.4hrs at pH 1) be the contrast of choice for chemoablation using acetic acid.

Real-time MRI guided catheter navigation

Co-registration of previously acquired CT or MRI three-dimensional volumes and/or electroanatomic maps can be used to enhance catheter positioning. But co-registration is subject to errors from respiration and cardiac motion, does not permit real-time monitoring of lesions, and cannot accommodate for geometric changes imparted by catheters and guidewires.

For device visualization in MRI, we relied on passive markers on the deflectable sheath and active visualization of the needle catheter to navigate and target chemoablation. Using real-time MRI, needle position was confirmed on orthogonal short and long axis planes through the LV. Future integration of needle catheters with MRI-conditional electroanatomic mapping systems may simplify this task.

Chemoablation lesion imaging

Correlation between lesion volumes by MRI and macroscopic volumes of injury has been evaluated for radiofrequency catheter ablation[3]. LGE best approximates macroscopic volumes of injury, but T2-weighted MRI overestimates and underestimates acute and chronic lesion volumes respectively. Although LGE may enable identification of radiofrequency lesions, it can only be performed once per procedure due to limitations in total gadolinium dose and cannot distinguish true necrotic core from edematous penumbra.

Insufficient or incomplete radiofrequency ablation likely explains current high recurrence rates after VT ablation.

Small volumes of gadolinium-containing solution can be visualized in real-time as they are injected into the myocardium using needle catheters. In this study, the volume of lesions immediately post-ablation correlated with the volume of LGE chronically. Extent of LGE correlates closely with volume of necrosis[28]. Chemoablation lesions that enhance on LGE correspond to areas of myocardial necrosis and fibrosis histologically. Radiofrequency lesion size can shrink by up to 50% chronically compared to immediately post-ablation. This phenomenon is likely caused by the reversible radiofrequency-induced edematous penumbra around the true necrotic core, which may impair the efficacy of repeated radiofrequency delivery. We did not observe this phenomenon with acetic acid lesions.

Isthmus ablation

Clinical usefulness of this technique depends on the ability to target specific tissues that can support VT. We demonstrate that real-time MRI permits precise targeting of chemoablation in an animal model of ischemic cardiomyopathy with an isthmus of normal myocardium between two areas of infarction. We demonstrate the ability to create a linear chemoablation lesion using multiple small injections confluent with the two infarcts, resulting in electroanatomic mapping confirmed disruption of the conductive isthmus.

Limitations

This was a preclinical feasibility study and we did not directly compare chemo- versus radiofrequency ablation. However, the limitations of radiofrequency ablation in the thick-walled LV are well recognized. Despite the advent of irrigation-tip catheters to enable longer ablations, needle-tip electrodes to facilitate deeper delivery of radiofrequency energy or contact force-sensing catheters to improve delivery of radiofrequency energy to the myocardium[29], procedural failures remain – almost certainly due to incomplete ablation. Porcine models of hemodynamically stable VT are difficult to create and for this reason we did not test ability of chemoablation to terminate arrhythmia. However, chemoablation did abolish late and fractionated electrograms within and around infarcted areas suggesting that critical substrate was eliminated. Recent data suggests that elimination of late potentials is at least as strong a predictor of freedom from VT in patients as non-inducibility[30, 31]. We did not test chemoablation within areas of dense or patchy scar. Further studies are needed to determine optimal injection volume, number of injections and distance from scar or grey zone in order to achieve arrhythmia termination while minimizing impact on ventricular function.

Equipping an MRI suite for interventional procedures requires additional infrastructure, including communication headsets, video projectors, and hemodynamic monitoring systems[19]. MRI injection catheters are not yet commercially available.

Many patients with VT have implantable cardioverter defibrillators that usually would disqualify them from undergoing MRI. MRI-conditional implants may permit MRI guided chemoablation, although implanted devices and leads can still cause imaging artifacts that

obscure target tissue and ablation lesions. These artifacts may be overcome with newer MRI pulse sequences[32].

Conclusion

This is the first report of real-time MRI guided transcatheter myocardial chemoablation. MRI enables instantaneous visualization of arrhythmic substrate and real-time monitoring of irreversible ablation lesions. Acetic acid creates more homogenous and well-circumscribed ablation lesions compared with ethanol. Unlike radiofrequency energy, endocardial needle chemoablation achieves fully transmural and irreversible ablation lesions, without edematous penumbra that may contribute to reversible conduction block and arrhythmia recurrence. We demonstrate feasibility of conductive isthmus ablation with abolition of local abnormal voltage activities in an animal model of ischemic cardiomyopathy. MRI guided chemoablation could improve procedural success of VT ablation.

Supplementary Material

Refer to Web version on PubMed Central for supplementary material.

Acknowledgments

We thank Robert S. Balaban for thoughtful comments; Joni Taylor and Katherine Lucas of the NHLBI Animal Surgery and Resources Core, and Stephanie French for technical help; St Jude Medical for electroanatomic mapping; and Innotom and Imricor for MRI-conditional deflectable sheaths.

Sources of Funding: Supported by the NHLBI, NIH (Z01-HL005062)

References

1. Kowalski M, Grimes MM, Perez FJ, Kenigsberg DN, Koneru J, Kasirajan V, Wood MA, Ellenbogen KA. Histopathologic characterization of chronic radiofrequency ablation lesions for pulmonary vein isolation. J Am Coll Cardiol. 2012; 59:930–938. [PubMed: 22381429]
2. Kolandaivelu A, Zviman MM, Castro V, Lardo AC, Berger RD, Halperin HR. Noninvasive assessment of tissue heating during cardiac radiofrequency ablation using MRI thermography. Circ Arrhythm Electrophysiol. 2010; 3:521–529. [PubMed: 20657028]
3. Harrison JL, Jensen HK, Peel SA, Chiribiri A, Grondal AK, Bloch LO, Pedersen SF, Bentzon JF, Kolbitsch C, Karim R, Williams SE, Linton NW, Rhode KS, Gill J, Cooklin M, Rinaldi CA, Wright M, Kim WY, Schaeffter T, Razavi RS, O'Neill MD. Cardiac magnetic resonance and electroanatomical mapping of acute and chronic atrial ablation injury: a histological validation study. Eur Heart J. 2014; 35:1486–1495. [PubMed: 24419806]
4. McGann C, Kholmovski E, Blauer J, Vijayakumar S, Haslam T, Cates J, DiBella E, Burgon N, Wilson B, Alexander A, Prastawa M, Daccarett M, Vergara G, Akoum N, Parker D, MacLeod R, Marrouche N. Dark regions of no-reflow on late gadolinium enhancement magnetic resonance imaging result in scar formation after atrial fibrillation ablation. J Am Coll Cardiol. 2011; 58:177–185. [PubMed: 21718914]
5. Bartlett TG, Mitchell R, Friedman PL, Stevenson WG. Histologic evolution of radiofrequency lesions in an old human myocardial infarct causing ventricular tachycardia. J Cardiovasc Electrophysiol. 1995; 6:625–629. [PubMed: 8535560]
6. Kramer JB, Saffitz JE, Witkowski FX, Corr PB. Intramural reentry as a mechanism of ventricular tachycardia during evolving canine myocardial infarction. Circ Res. 1985; 56:736–754. [PubMed: 3995700]

7. Estner HL, Zviman MM, Herzka D, Miller F, Castro V, Nazarian S, Ashikaga H, Dori Y, Berger RD, Calkins H, Lardo AC, Halperin HR. The critical isthmus sites of ischemic ventricular tachycardia are in zones of tissue heterogeneity, visualized by magnetic resonance imaging. Heart Rhythm. 2011; 8:1942–1949. [PubMed: 21798226]
8. Dukkipati SR, Mallozzi R, Schmidt EJ, Holmvang G, d'Avila A, Guhde R, Darrow RD, Slavin G, Fung M, Malchano Z, Kampa G, Dando JD, McPherson C, Foo TK, Ruskin JN, Dumoulin CL, Reddy VY. Electroanatomic mapping of the left ventricle in a porcine model of chronic myocardial infarction with magnetic resonance-based catheter tracking. Circulation. 2008; 118:853–862. [PubMed: 18678773]
9. Grothoff M, Piorkowski C, Eitel C, Gaspar T, Lehmkuhl L, Lucke C, Hoffmann J, Hildebrand L, Wedan S, Lloyd T, Sunnarborg D, Schnackenburg B, Hindricks G, Sommer P, Gutberlet M. MR imaging-guided electrophysiological ablation studies in humans with passive catheter tracking: initial results. Radiology. 2014; 271:695–702. [PubMed: 24484059]
10. Hilbert S, Sommer P, Gutberlet M, Gaspar T, Foldyna B, Piorkowski C, Weiss S, Lloyd T, Schnackenburg B, Krueger S, Fleiter C, Paetsch I, Jahnke C, Hindricks G, Grothoff M. Real-time magnetic resonance-guided ablation of typical right atrial flutter using a combination of active catheter tracking, passive catheter visualization in man: initial results from a consecutive patient series. Europace. 2015
11. Sigwart U. Non-surgical myocardial reduction for hypertrophic obstructive cardiomyopathy. Lancet. 1995; 346:211–214. [PubMed: 7616800]
12. Ellman BA, Parkhill BJ, Marcus PB, Curry TS, Peters PC. Renal ablation with absolute ethanol. Mechanism of action. Invest Radiol. 1984; 19:416–423. [PubMed: 6511249]
13. Baez-Escudero JL, Keida T, Dave AS, Okishige K, Valderrabano M. Ethanol infusion in the vein of Marshall leads to parasympathetic denervation of the human left atrium: implications for atrial fibrillation. J Am Coll Cardiol. 2014; 63:1892–1901. [PubMed: 24561151]
14. Baggish AL, Smith RN, Palacios I, Vlahakes GJ, Yoerger DM, Picard MH, Lowry PA, Jang IK, Fifer MA. Pathological effects of alcohol septal ablation for hypertrophic obstructive cardiomyopathy. Heart. 2006; 92:1773–1778. [PubMed: 16807273]
15. Brugada P, de Swart H, Smeets JL, Wellens HJ. Transcoronary chemical ablation of ventricular tachycardia. Circulation. 1989; 79:475–482. [PubMed: 2917386]
16. Tholakanahalli VN, Bertog S, Roukoz H, Shivkumar K. Catheter ablation of ventricular tachycardia using intracoronary wire mapping, coil embolization: description of a new technique. Heart Rhythm. 2013; 10:292–296. [PubMed: 23089899]
17. Wright KN, Morley T, Bicknell J, Bishop SP, Walcott GP, Kay GN. Retrograde coronary venous infusion of ethanol for ablation of canine ventricular myocardium. J Cardiovasc Electrophysiol. 1998; 9:976–984. [PubMed: 9786078]
18. Weismuller P, Mayer U, Richter P, Heieck F, Kochs M, Hombach V. Chemical ablation by subendocardial injection of ethanol via catheter–preliminary results in the pig heart. Eur Heart J. 1991; 12:1234–1239. [PubMed: 1782955]
19. Ratnayaka K, Faranesh AZ, Hansen MS, Stine AM, Halabi M, Barbash IM, Schenke WH, Wright VJ, Grant LP, Kellman P, Kocaturk O, Lederman RJ. Real-time MRI-guided right heart catheterization in adults using passive catheters. Eur Heart J. 2013; 34:380–389. [PubMed: 22855740]
20. Ohnishi K, Yoshioka H, Ito S, Fujiwara K. Prospective randomized controlled trial comparing percutaneous acetic acid injection and percutaneous ethanol injection for small hepatocellular carcinoma. Hepatology. 1998; 27:67–72. [PubMed: 9425919]
21. Greenbaum AB, Rogers T, Paone G, Flynn SE, Guerrero ME, O'Neill WW, Lederman RJ. Intentional Right Atrial Exit and Carbon Dioxide Insufflation to Facilitate Subxiphoid Needle Entry Into the Empty Pericardial Space: First Human Experience. JACC Clin Electrophysiol. 2015; 1:434–441. [PubMed: 26618198]
22. Cochet H, Komatsu Y, Sacher F, Jadidi AS, Scherr D, Riffaud M, Derval N, Shah A, Roten L, Pascale P, Relan J, Sermesant M, Ayache N, Montaudon M, Laurent F, Hocini M, Haissaguerre M, Jais P. Integration of merged delayed-enhanced magnetic resonance imaging and multidetector computed tomography for the guidance of ventricular tachycardia ablation: a pilot study. J Cardiovasc Electrophysiol. 2013; 24:419–426. [PubMed: 23252727]

23. Ashikaga H, Arevalo H, Vadakkumpadan F, Blake RC 3rd, Bayer JD, Nazarian S, Muz Zviman M, Tandri H, Berger RD, Calkins H, Herzka DA, Trayanova NA, Halperin HR. Feasibility of image-based simulation to estimate ablation target in human ventricular arrhythmia. Heart Rhythm. 2013; 10:1109–1116. [PubMed: 23608593]
24. Relan J, Chinchapatnam P, Sermesant M, Rhode K, Ginks M, Delingette H, Rinaldi CA, Razavi R, Ayache N. Coupled personalization of cardiac electrophysiology models for prediction of ischaemic ventricular tachycardia. Interface focus. 2011; 1:396–407. [PubMed: 22670209]
25. van Huls van Taxis CF, Wijnmaalen AP, Piers SR, van der Geest RJ, Schalij MJ, Zeppenfeld K. Real-time integration of MDCT-derived coronary anatomy and epicardial fat: impact on epicardial electroanatomic mapping and ablation for ventricular arrhythmias. JACC Cardiovasc imaging. 2013; 6:42–52. [PubMed: 23328560]
26. Sapp JL, Beeckler C, Pike R, Parkash R, Gray CJ, Zeppenfeld K, Kuriachan V, Stevenson WG. Initial human feasibility of infusion needle catheter ablation for refractory ventricular tachycardia. Circulation. 2013; 128:2289–2295. [PubMed: 24036605]
27. Yagishita D, Ajijola OA, Vaseghi M, Nsair A, Zhou W, Yamakawa K, Tung R, Mahajan A, Shivkumar K. Electrical homogenization of ventricular scar by application of collagenase: a novel strategy for arrhythmia therapy. Circ Arrhythm Electrophysiol. 2013; 6:776–783. [PubMed: 23873142]
28. Kim RJ, Fieno DS, Parrish TB, Harris K, Chen EL, Simonetti O, Bundy J, Finn JP, Klocke FJ, Judd RM. Relationship of MRI delayed contrast enhancement to irreversible injury, infarct age, and contractile function. Circulation. 1999; 100:1992–2002. [PubMed: 10556226]
29. Sohns C, Karim R, Harrison J, Arujuna A, Linton N, Sennett R, Lambert H, Leo G, Williams S, Razavi R, Wright M, Schaeffter T, O'Neill M, Rhode K. Quantitative magnetic resonance imaging analysis of the relationship between contact force and left atrial scar formation after catheter ablation of atrial fibrillation. J Cardiovasc Electrophysiol. 2014; 25:138–145. [PubMed: 24118197]
30. Vergara P, Trevisi N, Ricco A, Petracca F, Baratto F, Cireddu M, Bisceglia C, Maccabelli G, Della Bella P. Late potentials abolition as an additional technique for reduction of arrhythmia recurrence in scar related ventricular tachycardia ablation. J Cardiovasc Electrophysiol. 2012; 23:621–627. [PubMed: 22486970]
31. Jais P, Maury P, Khairy P, Sacher F, Nault I, Komatsu Y, Hocini M, Forclaz A, Jadidi AS, Weerasooryia R, Shah A, Derval N, Cochet H, Knecht S, Miyazaki S, Linton N, Rivard L, Wright M, Wilton SB, Scherr D, Pascale P, Roten L, Pederson M, Bordachar P, Laurent F, Kim SJ, Ritter P, Clementy J, Haissaguerre M. Elimination of local abnormal ventricular activities: a new end point for substrate modification in patients with scar-related ventricular tachycardia. Circulation. 2012; 125:2184–2196. [PubMed: 22492578]
32. Rashid S, Rapacchi S, Vaseghi M, Tung R, Shivkumar K, Finn JP, Hu P. Improved late gadolinium enhancement MR imaging for patients with implanted cardiac devices. Radiology. 2014; 270:269–274. [PubMed: 24086074]

WHAT IS KNOWN

- Contemporary electrophysiology techniques cannot visualize extent or continuity of radiofrequency energy ablation lesions, and struggle to achieve transmural ablation in the ventricular myocardium using endocardial and epicardial electrodes.

WHAT THE STUDY ADDS

- MRI guided myocardial chemoablation is a completely new approach that overcomes the fundamental limitations of radiofrequency ablation by enabling immediate depiction of irreversible and transmural lesions using endocardial needle catheters.
- Chemoablation with acetic acid creates more homogenous and well-circumscribed ablation lesions compared with ethanol.
- Unlike radiofrequency energy, endocardial needle chemoablation does not appear to cause an edematous penumbra that may contribute to reversible conduction block and arrhythmia recurrence.

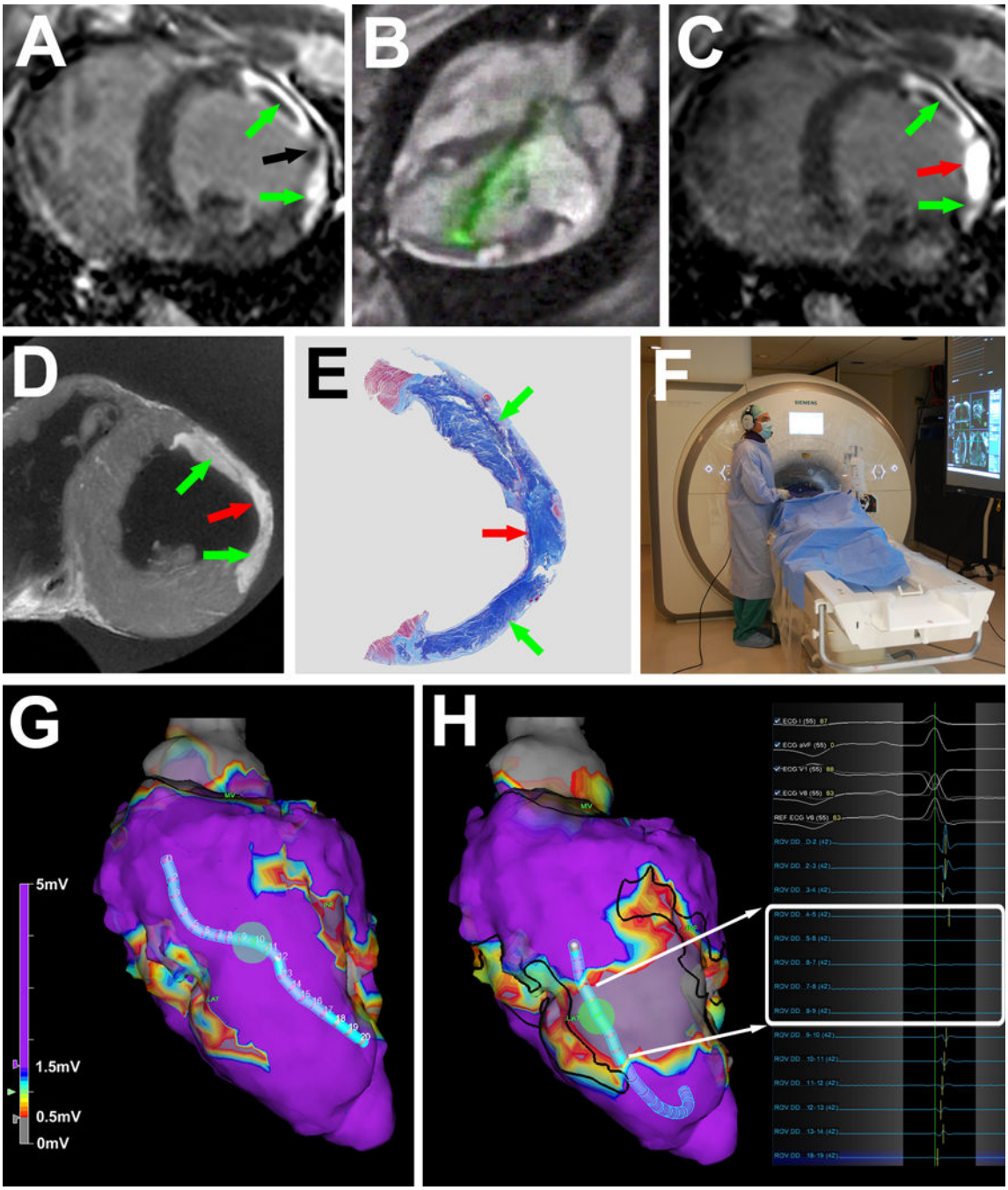

Figure 1.

MRI guided chemoablation of a conductive isthmus. (A) Baseline LGE showing two infarcts (green arrows) with isthmus of normal myocardium (black arrow). (B) Real-time MRI guided chemoablation. The active visualization injection needle appears in green. (C) LGE after chemoablation showing infarcts (green arrows) and transmural chemoablation lesion (red arrow). (D) After 7 days, ex-vivo high-resolution MRI confirms transmural chemoablation lesion (red arrow) confluent with both infarcts (green arrows). (E) Wide-field Masson trichrome stain of a section in the same orientation as panels A, C and D. Normal

myocardium appears pink, necrotic myocardium appears purple and fibrotic tissue appears blue. (F) The operator wears a noise-cancelling communications headset. Real-time MRI and hemodynamics are displayed in the room. (G) Endocardial voltage maps at baseline showing normal amplitude electrograms throughout the conductive isthmus. (H) Post-chemoablation, a band of very low (<0.5mV white box) voltages interrupts the isthmus. Black lines represent the margins of the original infarcts. LGE: late gadolinium enhancement.

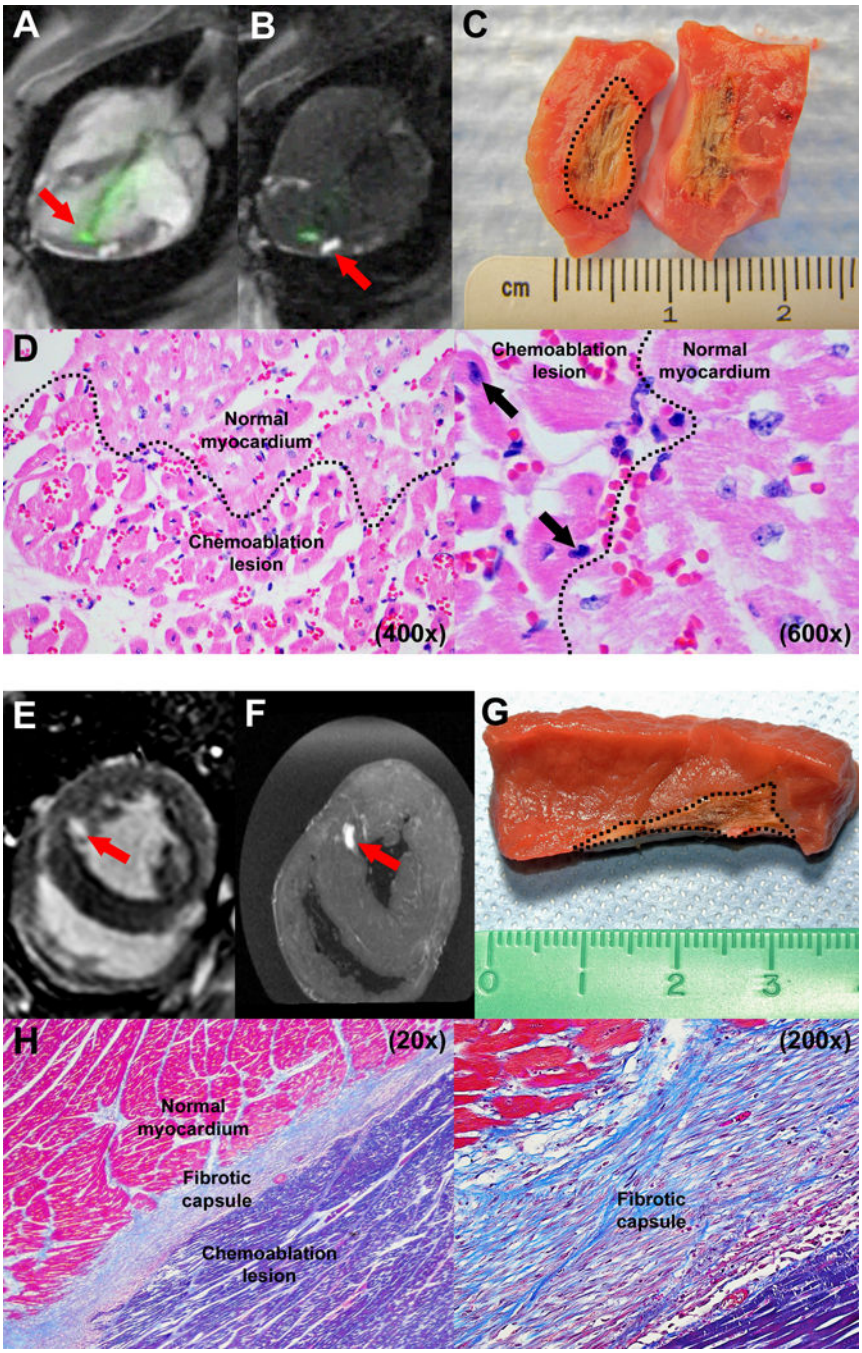

Figure 2.

Ablation imaging and histology. (A) Real-time MRI during chemoablation. The active visualization injection needle appears green (arrow). (B) Real-time inversion-recovery MRI darkens normal tissue and highlights chemoablation lesions containing gadolinium contrast (arrow). (C) Macroscopic appearance of an acute lesion, which has been butterflied open. The dotted line marks lesion margins. (D) Histology of acute lesion with H&E stains (400× and 600× magnification). Affected myocardial fibers are hypereosinophilic with pyknotic nuclei (black arrows). Dotted line marks border between chemoablation lesion and normal

myocardium. (E) Late gadolinium enhancement and (F) ex vivo MRI of a chronic lesion after systemic gadolinium contrast administration. (G) Macroscopically, chronic lesions have well circumscribed margins (marked with dotted line). (H) Histology of a chronic lesion with trichrome stain (20× and 200× magnification). Collagen stains blue, normal myocardial fibers stain red and necrotic myocardial fibers stain purple.

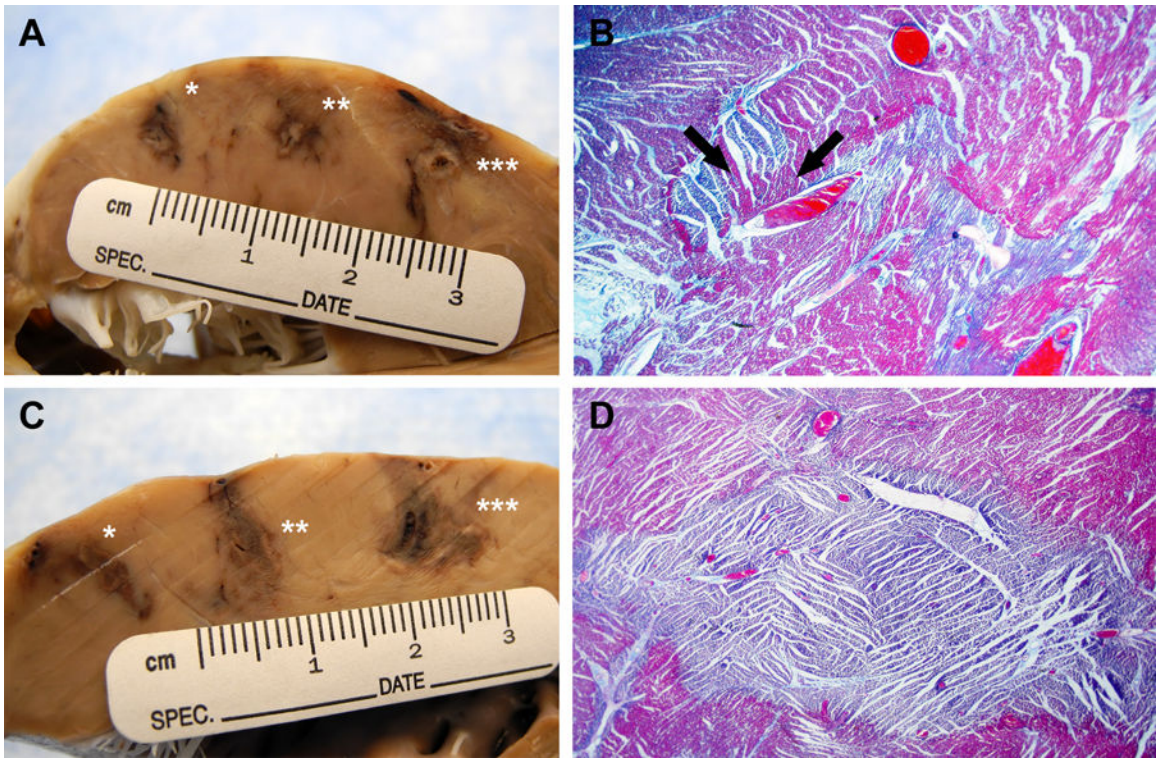

Figure 3.

Ethanol vs. acetic acid (A) Macroscopic appearance after fixing in formalin of 70% ethanol 0.2mL(*), 0.4mL(**) and 0.6mL(***) injections. (B) Trichrome stain of 0.6mL ethanol lesion (20× magnification). Lesion has stellate geometry with patchy areas of normal myocardium within the ablation field (black arrows). (C) Macroscopic appearance of 50% acetic acid 0.2mL(*), 0.4mL(**) and 0.6mL(***) injections. (D) Trichrome stain of 0.4mL acetic acid lesion (20× magnification). Lesion is homogeneous with well-circumscribed border.

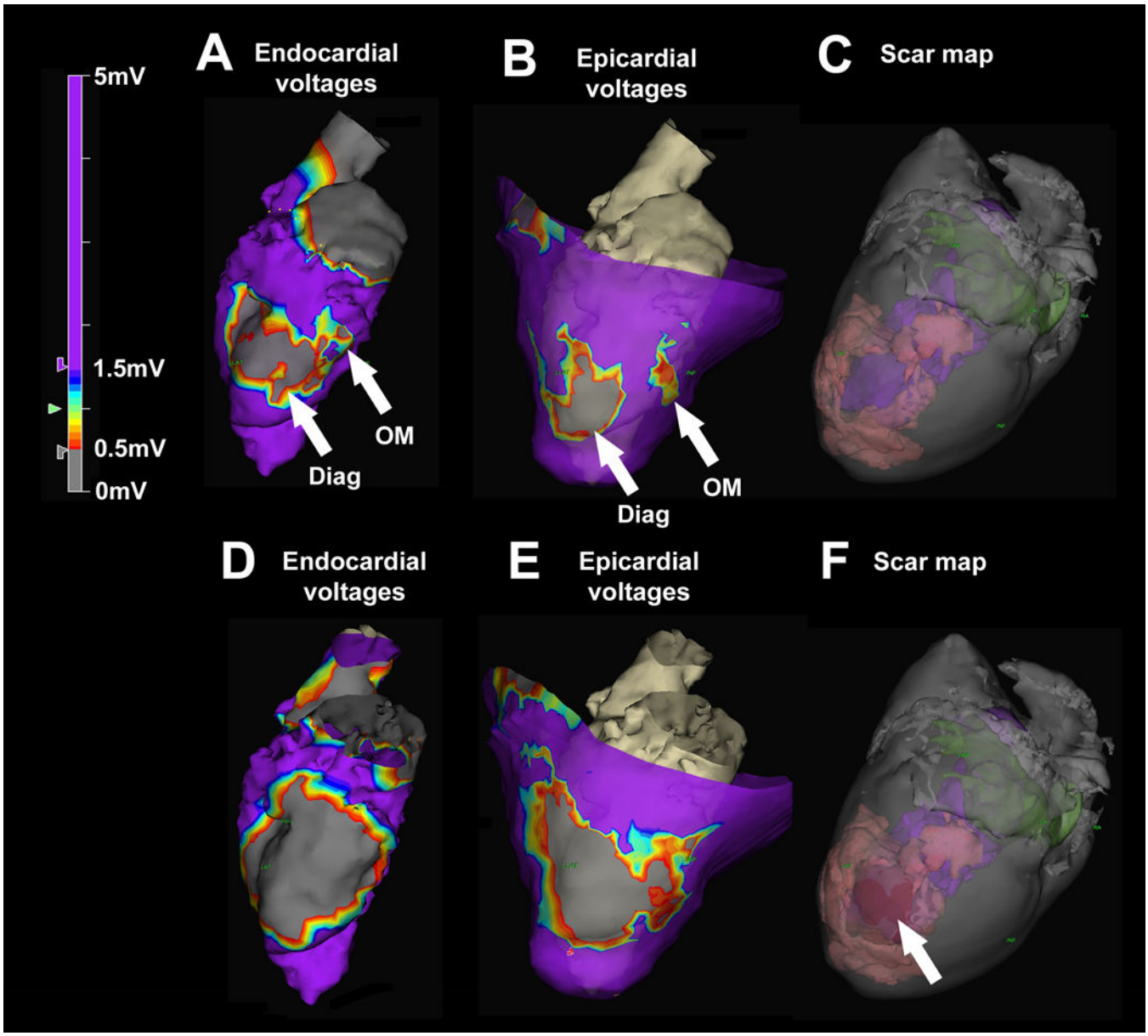

Figure 4.

Left ventricular endocardial electroanatomic mapping before and after chemoablation in an animal model of ischemic cardiomyopathy. (A) Baseline endocardial voltage map demonstrates low voltages corresponding with the diagonal infarct (Diag) and an adjacent heterogeneous area corresponding with the obtuse marginal infarct (OM). Purple represents normal voltages (>1.5mV) and grey represents very low voltages (<0.5mV). (B) Baseline epicardial map demonstrates two distinct areas of low voltage separated by an isthmus of normal conduction. (C) Baseline three-dimensional scar map derived from high-resolution ex-vivo MRI shows infarct (pink). The LV cavity appears in purple and the left atrium in green. (D) Post-chemoablation endocardial voltage map demonstrates low voltages with abolition of the heterogeneous area between the two infarcts. (E) Post-chemoablation

epicardial map confirmed interruption of the conductive isthmus. (F) The chemoablation lesion (arrow) appears in red and is confluent with the infarcts.

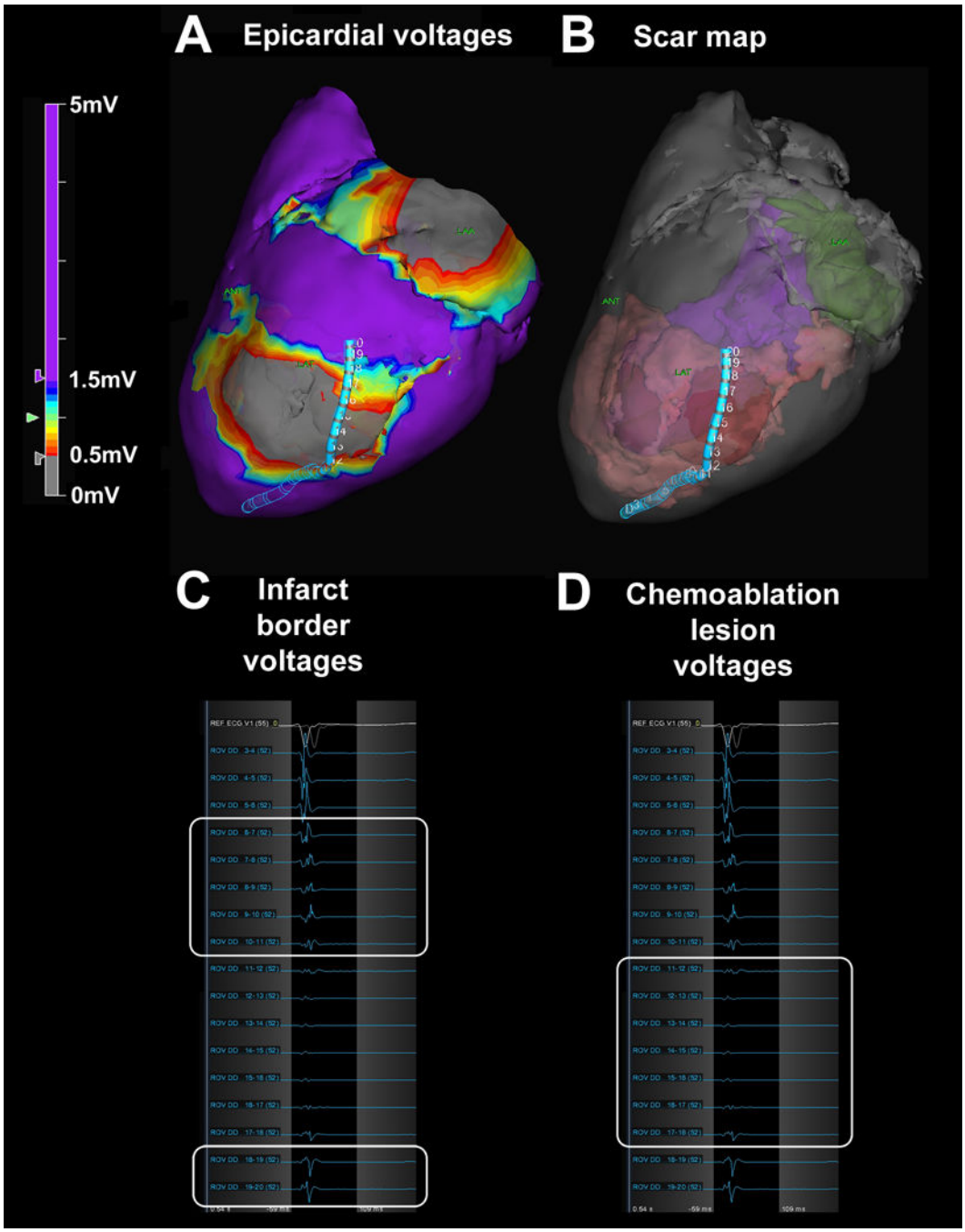

Figure 5.

Scar border geometry. (A) Epicardial voltage map showing the duo-decapolar mapping catheter spanning the chemoablation lesion. (B) Three-dimensional scar map derived from high-resolution ex-vivo MRI showing catheter position relative to pre-existing infarct (pink) and chemoablation lesion (red). The left ventricular cavity appears in purple and the left atrium in green. (C) Pre-existing infarct borders (white boxes) have low voltages (0.5–1.5mV), and (D) chemoablation lesion (white box) has extremely low voltages (<0.5mV).

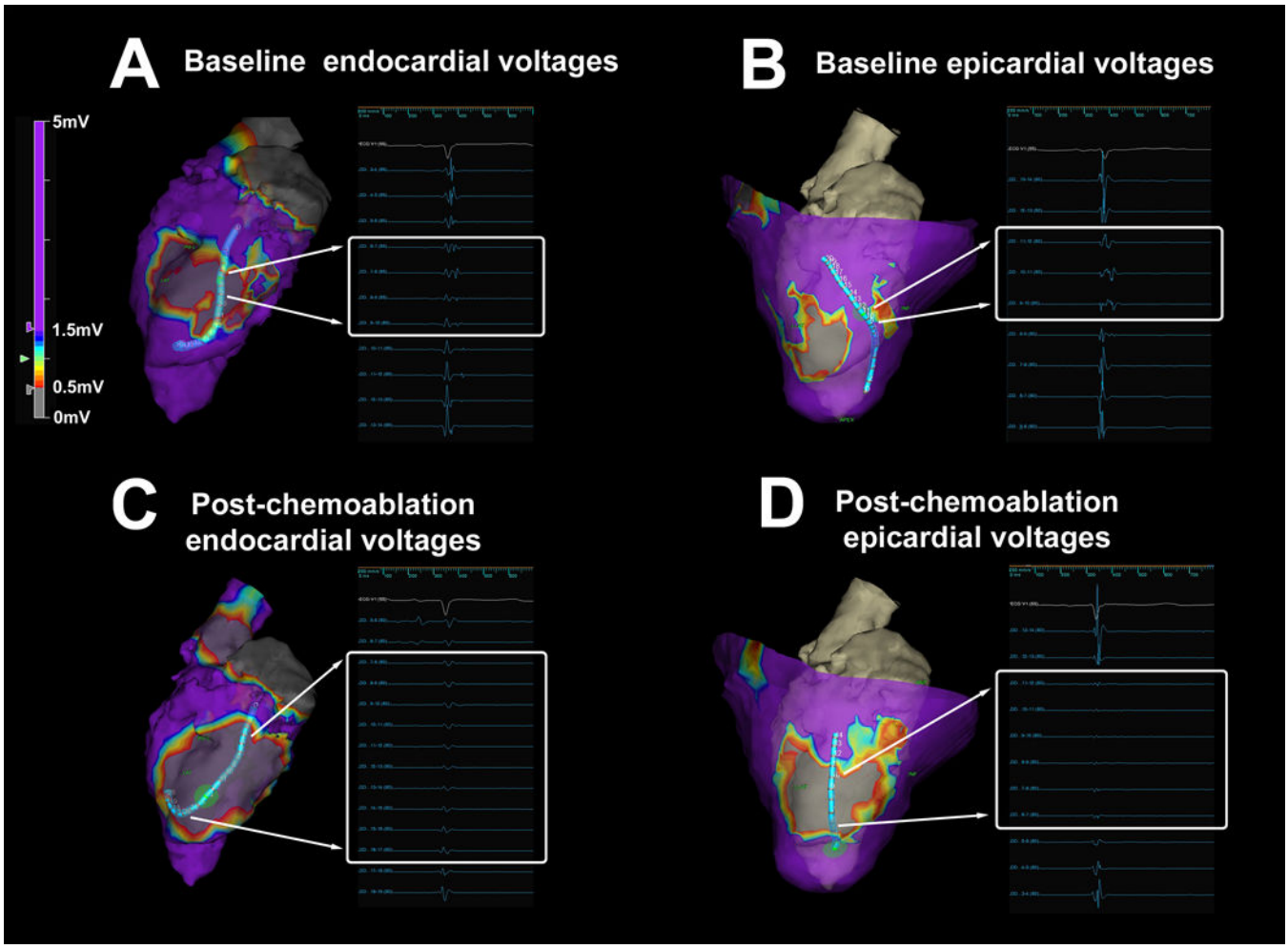

Figure 6.

Abolition of abnormal electrocardiograms with chemoablation. (A–B) At baseline, endocardial and epicardial mapping demonstrates local abnormal voltage activities (LAVA) with fragmented slow conduction between the infarcts. (C–D) After chemoablation, endocardial and epicardial mapping demonstrates abolition of LAVA and absence of far-field electrograms.